Curvature-induced bonding changes in carbon nanotubes investigated by electron energy-loss spectrometry

O. Stéphan,* P. M. Ajayan, and C. Colliex
Laboratoire de Physique des Solides, URA 002, Université Paris–Sud, Bâtiment 510, F-91405 Orsay cédex, France

F. Cyrot-Lackmann and É. Sandré
Laboratoire d'Études des Propriétés Électroniques des Solides–Centre National de la Recherche Scientifique, 25, rue des Martyrs, F-38042 Grenoble cedex 09, France

(Received 4 January 1996)

Effect of curvature-induced strain on the covalent bonding in isolated and selected single-shell and multi-shell carbon nanotubes is explored, using electron energy-loss spectroscopy (EELS) on the core *K* level, which probes the distribution of available unoccupied states in the conduction band. Results show that the curvature and mostly the layer stacking affect the σ^* conduction states. On the contratry, no influence is detected concerning the π^* band, even with corrugation angles up to 7° in a 1-nm-wide single-walled tube. First-principle local-density calculations are used to relate the features in the EELS spectra to the different atomic interactions in nanotubes. Finally, the covalent character of the bonding in existing nanotubes is discussed. [S0163-1829(96)00620-0]

I. INTRODUCTION

Before 1985, it was assumed that the only stable geometry for the threefold coordinated carbon atom was the graphite-like flat conformation. The discovery of new types of stable carbon structures [fullerenes, 1985 (Refs. 1,2); carbon-nanotubes 1991 (Refs. 3,4)] in which a finite curvature is imposed to the atomic threefold coordination has widened and revived the interest in studying the stability of carbon structures. Most of the cohesion in carbon aggregates is due to covalent bonding. Considering the carbon nanotube family, one can wonder how the threefold bonding depends on the curvature and how this influences our vision of the carbon bond in nanotubes.

As a consequence of the small dimensions of the concerned objects, a spectroscopy performed with a high degree of spatial resolution is required. electron energy-loss spectroscopy (EELS) combined with transmission electron microscopy provides spectra recorded from a typical (sub)nanometer area of a specimen, which can moreover be identified with imaging modes.[5] Core-edge features in EELS occur when a core electron is promoted to the unoccupied states above the Fermi level. In the present work, we investigate the excitation of carbon 1*s* electrons (*K* edge). Superimposed on the global edge profile, mostly governed by ineratomic considerations, are the ''energy-loss near-edge structures'' (ELNES), which reflect the sum of the different transition rates from the core state to all accesible states in the solid. They contain useful information about the atomic environment, such as the number of neighboring atoms, bond angles, and strain and local electronic states.[6,7] Each transition rate is separated into two components: the matrix element between the initial and the final state and the projected DOS. The energy-dependent shape of this fine structure is directly correlated to the density of the unoccupied conduction states, whereas the angular part of the matrix element determines the dependence on the scattering angle.[8]

In this paper, we first investigate the curvature-induced bonding changes in single-shell nanotubes (SSN) and multi-shell nanotubes (MSN) by EELS. Due to the restricted difference between the local coordination of the atoms in MSN and in bulk graphite, no clear change is observed in their respective EELS spectra: two bands are observed, which are attributed to transitions to the π^* and σ^* conduction bands. As for the SSN, although the curvature can no longer be neglected in the 1-nm-wide tubule, the π^* peak in the EELS spectra exhibits no detectable difference with the one in bulk graphite. On the contrary, the σ^* band partially loses its fine structure.

In order to interpret the experimental observations, *ab initio* band-structure calculations have then been performed on a corrugated graphite sheet, in which the carbon atoms are in a local coordination equivalent to that existing in the measured nanotubes. They show that this fine structure is partially related to the intersheet interactions in MSN. We finally conclude that for nanotubes as small as 1 nm wide, the covalent model is a satisfactory approach for describing the bonding.

II. EXPERIMENTAL CONSIDERATIONS

The carbon nanotubes have been obtained by carbon arc-discharge.[3] MSN found in the deposit of the cathode are made of concentric graphite cylinders, with an outer diameter ranging from 5 to 30 nm [see Fig. 1(a)].[3] On the other hand, SSN have been synthesized, using cobalt as a catalyst.[4] They are mostly packed into bundles, but some isolated SSN can be observed [see Fig. 1(b)]. In comparison to MSN, the SSN diameter is much smaller and is typically 1–2 nm.

In order to investigate the electronic structure of isolated nanotubes and to relate it to the detailed topography and nanostructure, a very local probe is needed. The carbon *K* core edges from isolated and selected SSN and MSN have been obtained using a scanning transmission electron microscope VG HB 501, equipped with a field-emission source and a parallel EELS spectrometer. This instrument produces

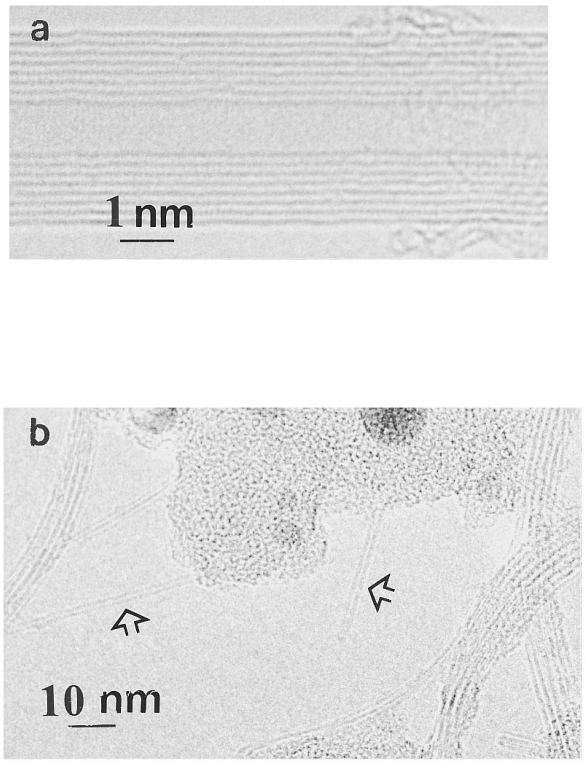

FIG. 1. (a) High-resolution image from a MSN made of eight rolled graphite walls. The external diameter is 6.5 nm. (b) Medium magnification image of bundles of SSN. Isolated SSN, similar to those investigated by EELS are arrowed.

EELS spectra with a typical 0.7-eV resolution recorded from subnanometer areas.[9] One can either fix the probe on a specific location or raster it over a reduced scan area while recording the corresponding spectrum. A new mode, called line-spectrum mode, improves the correlation between the spectral acquisition and the probe position on the specimen.[10] It consists of recording all the spectra, while ramping the probe with given steps across the specimen. Figure 2 shows a line spectrum acquired across a nanotube of 3-nm inner diameter and 10-nm outer diameter. The intensity of the carbon *K* edge, after background subtraction, follows the thickness profile. Furthermore, one can then address *a posteriori* any spectrum in the sequence, corresponding to a well-defined impact parameter with respect to the nanotubule section. In particular, the discrimination between spectra acquired in the center and on the rim of a tube becomes obvious.

Acquisition times required for achieving a satisfactory signal-to-noise level on any spectrum are of the order of a few seconds when the thickness is of the order of 10 nm. For SSN of much reduced thickness, therefore producing spectra of much lower intensity, we have also kept an acquisition time of a few seconds in order to avoid radiation-induced structural damage. A previous scanning transmission electron microscopy study had revealed large shape transformations in single-shell carbon nanotubes: after several seconds the SSN walls were seen waving and breaking under the beam.[11] During the present investigation, the monotube shape has been checked after each EELS measurement to be sure that the SSN spectrum is typical of a non highly modified SSN with straight walls and no amorphous carbon coating it.

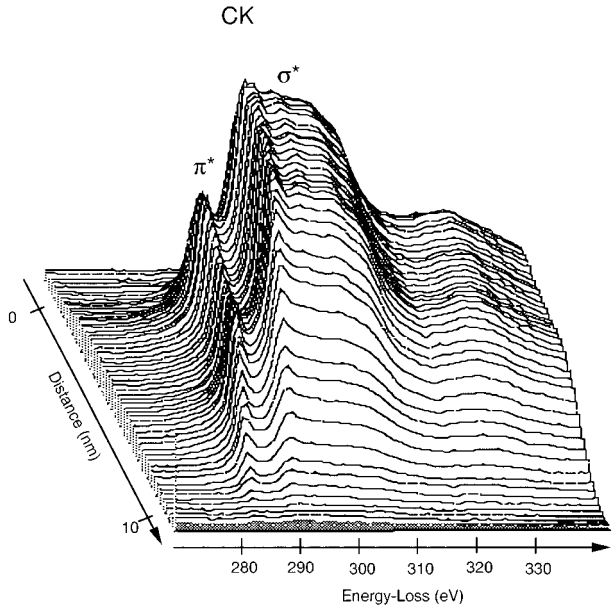

FIG. 2. Line spectrum across a multiwalled carbon nanotube of 10-nm outer diameter, displaying the evolution of the carbon *K*-edge fine structures, as the subnanometer incident probe is scanned across it.

III. RESULTS

A. Multishell nanotubes

The tube axis is set perpendicularly to the electron beam. Two different spectra are selected corresponding to two probe positions: a central position, where the **c** axis is parallel to the beam and an edge position, where it is perpendicular to the beam (Fig. 3). For comparison we have also introduced in the same figure a representative spectrum for a typical graphite crystal. Because of the almost flat conformation of the threefold coordinated atoms in wide carbon nanotubes, both graphite and MSN exhibit identical ELNES features.[12,13] The sharp peak at 285.5 eV is due to transitions from the 1*s* core level to the π^* band and the band starting at 291 eV corresponds to transitions to the *p*-orbital projected part (because of the dipole selection rule valid for the small scattering angles used in this experiment, up to 15 mrad for incident electrons of 100 keV) of the broad σ^* band.[14,15] The local anisotropy in MSN is clearly pointed out by the changes in the intensity ratio π^*/σ^*, which is larger for the edge position than for the central position (in our scattering geometry, the mean momentum transfer is perpendicular to the beam, see Fig. 3). Such a difference has been reported in graphite for grazing and normal incidence.[13] Because of the very small curvature, which is imposed to the atomic coordination in wide nanotubes (0.5° for a 25-nm-wide nanotube), there should be no difference between the bond in MSN and in bulk graphite. Indeed, no difference is experimentally found.

B. Single-shell nanotubes

In a 1-nm-wide SSN, the bending angle (deviation from the planar conformation) is around 7° and can no longer be

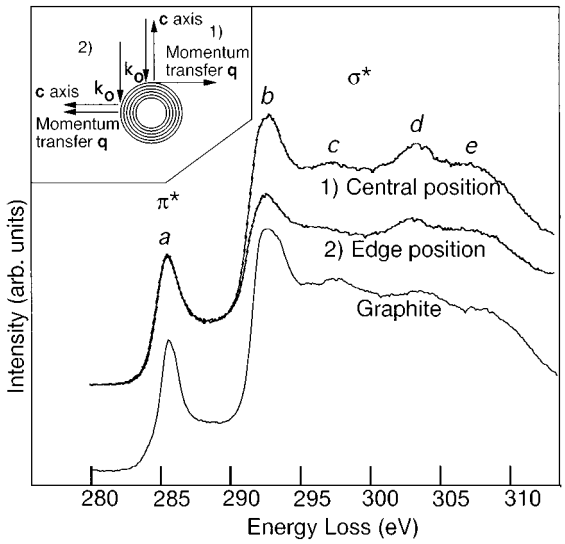

FIG. 3. ELNES on carbon *K* edges from MSN for two probe positions (1) and (2), respectively, in the center and on the rim. The scattering geometry used in our EELS experiment is displayed in inset.

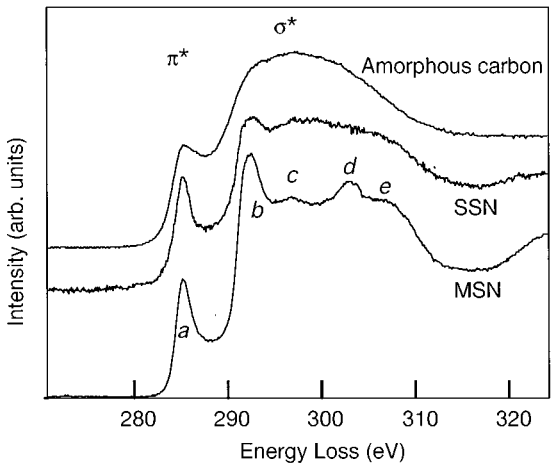

FIG. 4. Carbon *K*-edge ELNES on a 30-nm-diameter MSN compared with that on a 1-nm-diameter SSN. The dispersion per channel is 0.05 eV. For reference, ELNES from amorphous carbon is given and exhibits a wider π^* peak.

neglected. However, no difference is observed in the π^* peaks recorded from both SSN and MSN. On the contrary, the σ^* parts in the ELNES recorded from a SSN and from a MSN exhibit important differences. From the four main peaks in the MSN spectrum, only two remain in the SSN spectrum; peak *b* broadens; the three other ones are replaced by a broad resonance, which exhibits a maximum somewhere in between the positions of peaks *c* and *d* in the MSN spectrum. The ELNES of the 30-nm-wide MSN and of the 1-nm-wide SSN are compared in Fig. 4. The experimental fact that the π^* remains unchanged when the curvature increases from MSN to SSN is in contradiction with previous measurements from bundles of SSN, where a broadening of the π^* peak was interpreted as due to the curving of the sheets.[16] From our results, it seems that this broadening is due to the presence of amorphous carbon in the bundles (see the spectrum for amorphous carbon also shown in Fig. 4 for comparison).

IV. DISCUSSION

In the literature, the bonding in nanotubes is often postulated as covalent.[17] Following Pauling,[18] the covalent bond is defined as the sharing of a pair of electrons by the two bonded atoms. In other terms, covalency is characterized by the localized and directional character of the electronic wave functions. Generally speaking, a solid is covalently bonded if the whole structure energy stabilization can be written as the sum of local energy terms in the two-center first-neighbor scheme:

$$E_{\text{stabilization}} = \sum_{\substack{i,j \\ \text{first neighbors}}} E_{\text{bonding}}(i,j). \qquad (1)$$

The covalent bond is opposed to the metallic bond for which the most striking character is the mobility of the bonding electrons. If postulating the covalent character of the bonding in nanotubes, long-range ordering should not influence the number and the position of the main peaks in the conduction band. Such a covalent description has been shown to be correct considering graphitelike coordinated carbon structures. On the contrary, considering very narrow nanotubes, it has been shown that the curvature modifies drastically the nature of the valence bond: based on LDA calculations, Blase *et al.*[19] have recently reported the large hybridization of the π^* and σ^* bands of the graphite sheet network in small radius ''sawtooth'' nanotubes,[20] with diameter inferior to 7 Å. This strong hybridization induces a drastic modification of the energy and of the character of the lowest-lying conduction band in extremely narrow nanotubes: although wide sawtooth tubes are predicted to be large gap semiconductors, tubes with diameter inferior to 4.8 Å are shown to be metallic. In practice, only nanotubes with diameter superior to 1 nm are available. In this paper, we first postulate that the bonding remains mainly covalent in real carbon nanotubes. If the bonding is covalent, two structures, in which the carbon atoms are in identical local coordination, should exhibit identical features in their respective ELNES or conduction bands. Though the structure of nanotubes is complex, the first-neighbor atomic coordination is identical in nanotubes and in corrugated graphite.[15] In the following lines, we interpret the effect of curvature induced bonding in nanotubes by investigating the corrugation induced bonding in isolated graphite sheets (graphene).

Since the position of the different peaks is mainly dependent on the density of antibonding states, and since their respective width is unaffected by the anisotropy in graphite,[12,13] we are entitled to compare the experimental MSN and SSN ELNES structures with calculated *p*-orbital projected densities of conduction states (*p*-DOS). All the different *p*-DOS, which are presented in this paper, are calculated using the first-principle LMTO-ASA method (linear muffin-tin orbital within the atomic sphere approximation).[21] We have used a scalar relativistic code (neglecting spin-orbit coupling) for which the density-functional formalism was treated within the local-density approximation (LDA), using von Barth and Hedin exchange and correlation potential.[22]

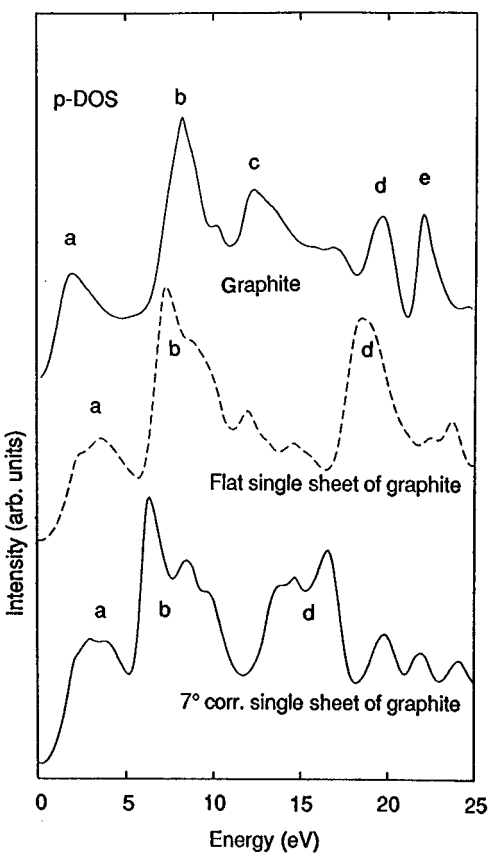

FIG. 5. LMTO calculated p-DOS for graphite, compared to those for a flat and a 7° corrugated graphene layer.

The basis function for the calculations included all angular momentum up to $l=2$. Carbon sphere states were chosen to be $2s$, $2p$, and $3d$, and empty sphere states were chosen as $1s$, $2p$, and $3d$. A set of four independent empty spheres associated with two independent carbon spheres were considered to describe graphite structures as it is required by the ASA. The DOS were calculated considering a set of more than one thousand nonequivalent k points. A 0.5-eV Gaussian function was used to smooth the calculated DOS in order to remove all structures with sizes inferior to the resolution of our EELS spectrometer (0.7 eV). The influence of the slab stacking on the conduction state peak positions was estimated by calculating the density of states for both stable graphite phases: trigonal (ABC stacking) and hexagonal (AB stacking) graphite. No difference in the peak positions is seen showing that the different peaks are related to the inner plane coordination and/or to the first-neighbor slab interactions only. When comparing the experimental graphite ELNES features (see Fig. 3) and the LMTO calculated p-DOS for graphite (see Fig. 5), they are in very good agreement.

The electronic structure of both flat and corrugated graphene (one monolayer of hexagonally coordinated carbon atoms) are calculated considering a supercell imposing an interslab distance of 6.7 Å. In order to restore compacity, we consider a set of ten empty spheres and two carbon spheres. The agreement between experimental measurements on nanotubes (see Fig. 4) and theoretical calculations on corrugated graphite (Fig. 5) lead us to conclude that the bonding in real nanotubes is mainly covalent, as evidenced below.

TABLE I. Transfer integrals for corrugated graphene.

$$\beta_{p_xp_x}=\beta_{p_yp_y}=\left[1+\frac{\cos^2(\theta)}{2}\right]V_{pp\sigma}+\left[2-\frac{\cos^2(\theta)}{2}\right]V_{pp\pi}$$

$$\beta_{sp_x}=0 \qquad \beta_{sp_y}=0 \qquad \beta_{sp_z}=3\sin(\theta)V_{sp\sigma}$$

$$\beta_{ss}=3V_{ss\sigma} \qquad \beta_{p_xp_y}=\beta_{p_yp_x}=0$$

$$\beta_{p_zp_z}=3[\cos^2(\theta)V_{pp\pi}+\sin^2(\theta)V_{pp\sigma}]$$

We will first be concerned with the difference in the σ^* bands between the ELNES obtained with SSN and MSN. Since these bands are far above the Fermi level, a full electron method like the LMTO-ASA is required. Comparing the density of states of graphite (interslab distance of 3.35 Å) and of graphene (calculation performed on a 6.7 Å interslab distance graphite), it is found that the interplane interaction is partially responsible for the MSN graphitelike σ^* band structure (see Fig. 5). Peaks c and e in the bulk graphite p-DOS do not appear in the graphene p-DOS. They result from the interaction between two adjacent slabs. Finally, comparing the flat and 7° corrugated graphite slabs, we measure the effect of curvature on the σ^*: as seen in Fig. 4, both peaks b and d broaden and peak d is shifted to lower energies. This is in accordance with the change in the ELNES when going from the MSN to the SSN (Fig. 4).

Let us now concentrate on the experimental invariance of the π^* peak width (W) with the curvature. Both *ab initio* and semiempirical Tight-binding (TB) approaches are used to relate this experimental fact to a theoretical vision of the covalent bond in nanotubes. Though *ab initio* self-consistent calculations are more reliable and hence must be used to check any theoretical development, a semiempirical modeling of the band structure provides an elementary and direct relation between the physical properties and the crystal structure. In a previous study,[15] we have investigated the accuracy of the two-center first-neighbor (TB) scheme in describing the bonding changes in corrugated graphite. In Ref. 15, it is shown that, whatever the coordination curvature, the π^* bandwidth is always determined by real-space interactions (center of the first Brillouin-zone energetic relations). The width of the π^* band in the corrugated graphite sheet (W) is then given by

$$W=\frac{E_\pi^*(\mathbf{k}=\mathbf{0})-E_\pi(\mathbf{k}=\mathbf{0})}{2}, \tag{2}$$

where E_π ($\mathbf{k}=\mathbf{0}$) [respectively, E_π^* ($\mathbf{k}=\mathbf{0}$)] is the π state energy at the center of the first Brillouin zone (respectively, π^* state energy). In a planar sheet of graphite, since p_z orbitals are decoupled from other orbitals, the π/π^* state energy reduces to the sum of the site energy E_{p_z} with the transfer integral $\beta_{p_zp_z}$. In corrugated graphite, the curvature in the local coordination induces a coupling between s and p_z orbitals. The Fermi-level eigenvalue problem is made complicated by the introduction of β_{sp_z} and β_{ss} transfer integrals and has then no exact solution. However, we can easily determine the interval to which E_π^* ($\mathbf{k}=\mathbf{0}$) and E_π ($\mathbf{k}=\mathbf{0}$) belong. Using the expressions from Ref. 23 of the different transfer integrals β_{sp_z}, β_{ss}, $\beta_{p_zp_z}$, introducing the bending angle, we deduce the analytical formulation of the different transfer integrals in corrugated graphene (Table I). Introduc-

TABLE II. Transferable Slater-Koster parameters for carbon. The energies are expressed in eV.

E_s	E_p	V_{sss}	V_{sps}	V_{pps}	$V_{pp\pi}$
−7.5	0	−5	5	5	−2

ing these expressions in the energetic characteristic equation, we get the following limits for W:

$$\{3|V_{pp\pi}|-3\sin^2(\theta)[V_{pp\sigma}-V_{pp\pi}]\}\times\left(1-3\tan^2(\theta)\frac{V_{sp\sigma}^2}{V_{pp\pi}}\frac{1}{|(E_{p_z}-E_s)-3(V_{pp\pi}+V_{ss\sigma})|}\right)\leqslant W\leqslant\{3|V_{pp\pi}|-3\sin^2(\theta)[V_{pp\sigma}-V_{pp\pi}]\},\quad(3)$$

where E_s is the s-orbital site energy, E_{p_z} is the p_z-orbital site energy, $V_{ss\sigma}$, $V_{sp\sigma}$, $V_{pp\sigma}$, $V_{pp\pi}$ are the Slater-Koster (SK) parameters.[23] They are the minimum number of transfer integrals to be considered in a carbon atom based structure. The SK parameters do not depend on the coordination, but only on the interatomic distance. A proper numerical set of SK parameters is gathered in Table II and leads to the numerical interval:

$$[6-21\sin^2(\theta)][1-(0.69)\tan^2(\theta)]\leqslant W\leqslant[6-21\sin^2(\theta)].\quad(4)$$

For a 1-nm-wide SSN, the curvature angle (θ) is about 7°. The corresponding π^* bandwidth change is then estimated as

$$W(7°)-W(0°)=0.3\ \text{eV},$$

while

$$W(0°)=6\ \text{eV}.\quad(5)$$

W(7°)–W(0°) has to be compared with the energy accuracy of our EELS measurements, i.e., 0.7 eV. Consequently, from the above TB calculations, no noticeable difference is expected in the π^* bandwidth when comparing the ELNES of the MSN and the SSN. This result is consistent with the first-principle LMTO-ASA calculations performed on a flat and on a 7° corrugated graphite planes (Fig. 5).

V. CONCLUSION

Electron energy-loss spectroscopy has been used to perform accurate measurements of electron states on well-identified isolated carbon nanotubes. The near-edge structure on the carbon K edge can then be compared when recorded from multiwalled tubes with diameter between 5 and 20 nm or from single-walled tubes with a diameter of the order of 1 nm. Since we have shown that two structures (curved graphene and corrugated graphene), in which the atoms are in identical coordination, exhibit the main features in their respective DOS, the covalent character of the bonding in wide enough nanotubes (with bending angle $\theta\leqslant 7°$) has been confirmed. The main features in the ELNES of the 1-nm-wide nanotubes well correspond to the main features in the p-DOS of the corrugated graphene. Considering only real-space interactions in a tight-binding approach, we can justify the absence of modification of the π^* band when curvature increases from the large MSN to the 1-nm-wide SSN. However, *ab initio* calculations are required to demonstrate that the σ^* fine structures of MSN are partially due to interactions between different sheets (peaks c and e) and that the position of peak d is curvature dependent.

ACKNOWLEDGMENTS

One of the author (P.A.) thanks the CNRS departments SPM and SC for granting him during his stay at the Orsay LPS laboratory. This study has been performed with the support of the CNRS Ultimatech interdisciplinary program.

*Author to whom correspondence should be addressed.

[1] H. W. Kroto, J. R. Heath, S. C. O'Brien, R. F. Curl, and R. E. Smalley, Nature **318**, 162 (1985).

[2] W. Krätschmer, L. D. Lamb, K. Foristopoulos, and D. R. Huffman, Nature **347**, 354 (1990).

[3] S. Iijima, Nature **354**, 56 (1991); T. W. Ebbesen and P. M. Ajayan, *ibid*. **358**, 220 (1992); S. Iijima and T. Ichihashi, *ibid*. **363**, 603 (1993).

[4] D. S. Bethune, C. H. Kiang, M. S. deVries, G. Gorman, R. Savoy, J. Vazquez, and R. Beyers, Nature **363**, 605 (1993); P. M. Ajayan, J. M. Lambert, P. Bernier, L. Barbedette, C. Colliex, and J. M. Planeix, Chem. Phys. Lett. **215**, 509 (1992).

[5] C. Colliex, in *Transmission Electron Energy Loss Spectrometry in Materials Science*, edited by M. M. Disko, C. C. Ahn, and B. Fultz, The TMS Monographs Series Vol. 2 (Minerals, Metals, and Materials Society, Warrendale, PA, 1992), p. 85.

[6] C. Colliex, T. Manoubi, M. Gasgnier, and L. M. Brown, Scanning Electron Microsc. **2**, 489 (1985).

[7] X. Weng, P. Rez, and H. Ma, Phys. Rev. B **40**, 4175 (1989).

[8] R. D. Leapman and J. Silcox, Phys. Rev. Lett. **42**, 1361 (1979).

[9] D. Bouchet, C. Colliex, P. Flora, O. Krivanek, C. Mory, and M. Tencé, Microsc. Microanal. Microstruct. **1**, 443 (1990).

[10] C. Colliex, M. Tencé, E. Lefèvre, C. Mory, H. Gu, D. Bouchet, and C. Jeanguillaume, Mikrochim. Acta **114/115**, 71 (1994).

[11] P. M. Ajayan, C. Colliex, P. Bernier, and J. M. Lambert, Microsc. Microanal. Microstruct. **4**, 501 (1993).

[12] P. E. Batson, Phys. Rev. B **48**, 2608 (1993).

[13] R. A. Rosenberg, P. J. Love, and V. Rehn, Phys. Rev. B **33**, 4034 (1986).

[14] J. C. Charlier, X. Gonze, and J. P. Michenaud, Phys. Rev. B **43**, 4569 (1991).

[15] E. Sandré, J. P. Julien, and F. Cyrot-Lackmann, J. Phys. Chem. Solids **55**, 1268 (1994).

[16] R. Kuzuo, M. Terauchi, M. Tanaka, and Y. Saito, Jpn. J. Appl. Phys. **33**, L1316 (1994).

[17] A. A. Lucas, P. H. Lambin, and R. E. Smalley, J. Phys. Chem. Solids **54**, 587 (1993); S. Sawada and N. Hamada, Solid State Commun. **83**, 917 (1992).

[18] L. Pauling, *The Nature of The Chemical Bond* (Cornell University Press, Ithaca, New York, 1960).

[19] X. Blase, L. X. Benedict, E. L. Shirley, and S. G. Louie, Phys. Rev. Lett. **72**, 1978 (1994).

[20] J. W. Mintmire, B. I. Dunlap, and C. T. White, Phys. Rev. Lett. **68**, 631 (1992); N. Hamada, S. Sawada, and A. Oshiyama, *ibid*.

68, 1579 (1992); R. Saito, M. Fujita, G. Dresselhaus, and M. S. Dresselhaus, Appl. Phys. Lett. **60**, 2204 (1992).

[21] O. K. Andersen, Phys. Rev. B **12**, 3060 (1975); O. K. Andersen, O. Jepsen, and D. Glötzel, in *On Highlights of Condensed Matter Theory*, edited by F. Bassani, F. Fumi, and M. P. Tosi (North-Holland, New York, 1985).

[22] U. von Barth and L. Hedin, J. Phys. C **5**, 1629 (1965).

[23] J. C. Slater and G. F. Koster, Phys. Rev. **94**, 1498 (1954).